International Journal of Nanomedicine

Dovepress
open access to scientific and medical research

Open Access Full Text Article

ORIGINAL RESEARCH

# PEGylated Graphene Oxide Carried OH-CATH30 to Accelerate the Healing of Infected Skin Wounds



Di Mei[1,*]
Xiaolong Guo[2,*]
Yirong Wang[1]
Xiaofei Huang[1]
Li Guo[1]
Pengfei Zou[3]
Delong Ge[1]
Xinxin Wang[1]
Wenhui Lee[4]
Tongyi Sun[1]
Zhiqin Gao[1]
Yuanyuan Gao[3]

[1]School of Life Science and Technology, Shandong Key Laboratory of Proteins and Peptides Pharmaceutical Engineering, Shandong Universities Key Laboratory of Biopharmaceuticals, Weifang Medical University, Weifang, Shandong, 261053, People's Republic of China; [2]School of Basic Medicine, Weifang Medical University, Weifang, Shandong, 261053, People's Republic of China; [3]School of Pharmacy, Weifang Medical University, Weifang, Shandong, 261053, People's Republic of China; [4]Key Laboratory of Animal Models and Human Disease Mechanism, Institute of Zoology, Kunming, Yunnan, 650233, People's Republic of China

*These authors contributed equally to this work

**Background:** The treatment of *Staphylococcus aureus* (*S. aureus*)-infected wounds is difficult. It causes extreme pain to tens of thousands of patients and increases the cost of medical care. The antimicrobial peptide OH-CATH30 (OH30) has a good killing activity against *S. aureus* and can play a role in accelerating wound healing and immune regulation. Therefore, it shows great potential for wound healing.

**Purpose:** The aim of this study was to overcome the short half-life and easy enzymolysis of OH30 by using graphene oxide conjugated with polyethylene glycol to load OH30 (denoted as PGO-OH30), as well as to evaluate its effect on wounds infected by *S. aureus*.

**Methods:** PGO-OH30 nanoparticles were prepared by π–π conjugation and characterized. Their cell cytotoxicity, cell migration, infectious full-thickness dermotomy models, and histopathology were evaluated.

**Results:** Characterization and cytotoxicity experiments revealed that the PGO-OH30 drug-delivery system had good biocompatibility and excellent drug-delivery ability. Cell-migration experiments showed that PGO-OH30 could promote the migration of human immortalized keratinocytes (HaCaT) cells compared with the control group ($P<0.05$). In a mouse model of skin wound infection, PGO-OH30 accelerated skin-wound healing and reduced the amount of *S. aureus* in wounds compared with the control group ($P<0.05$). In particular, on day 7, the number of *S. aureus* was 100 times lower in the PGO-OH30 group than in the control group.

**Conclusion:** The PGO-OH30 drug-delivery system had good biocompatibility and excellent drug-delivery ability, indicating its good therapeutic effect on a skin wound-infection model.

**Keywords:** OH-CATH30, bacterial infection, graphene oxide, skin wound

Correspondence: Zhiqin Gao
School of Life Science and Technology, Shandong Key Laboratory of Proteins and Peptides Pharmaceutical Engineering, Shandong Universities Key Laboratory of Biopharmaceuticals, Weifang Medical University, Weifang, Shandong, 261053, People's Republic of China
Tel +86 5368462066
Email zhiqingao2013@163.com

Yuanyuan Gao
School of Pharmacy, Weifang Medical University, Baotong Road, Weifang, Shandong Province, 261053, People's Republic of China
Tel +86 536 846 2067
Email yyg20062006@126.com

## Introduction

Skin has the function of preventing pathogens from entering the body. Skin damage, including those acquired from mechanical injuries, surgeries, and sports, is very common in our daily life[1,2] and can cause discomfort. Any form of skin injuries can disrupt this barrier function of the skin,[3,4] and damaged skin is more susceptible to bacterial attack.[5] *S. aureus* infection in skin wounds has serious consequences. Bacteria in wounds produce various cytotoxins during reproduction, leading to increased levels of inflammation, followed by tissue necrosis and other reactions that can slow the healing of normal wounds or even cause systemic infection and shock.[6–8] Skin-wound infections cause extreme pain to clinical patients and increase the cost of medical treatment.[9–11] Thus, antibacterial treatment at the

Received: 6 February 2021
Accepted: 20 June 2021
Published: 13 July 2021

wound site is very important.[12,13] Antibiotics are often used clinically to fight bacterial infections in wounds. However, the widespread use and even abuse of antibiotics have led to the emergence of various drug-resistant bacteria and superbug in clinical practice.[14,15] The side effects of antibiotics have also caused many adverse reactions in people.[16,17] Due to the lack of effective antibiotic treatment, the mortality caused by drug-resistant bacterial infections increases yearly. The cost of treatment is also rising, thereby threatening to clinical patients and posing new challenges to clinical antimicrobial treatment.[18,19]

The abuse of antibiotics leads to continuously increased of bacterial resistance, so the substitution of antibiotics is particularly urgent and has been well studied over the past few decades.[20,21] Antimicrobial peptides exist widely in nature and are an important part of the innate immune system of most animals and plants.[22] Owing to the wide-ranging antibacterial activity and low drug resistance of antimicrobial peptides, they are considered as the best substitute for antibiological agents.[23,24] A cationic antimicrobial peptide from the king cobra, OH30 has extensive antibacterial activity, promotes skin wound healing, and has anti-inflammatory and immune-regulation activities, among other functions.[25–27] The therapeutic potential of AMPs has been actively studied in many bacterial infections, including skin infections, pneumonia, and peritonitis.[28] However, natural polypeptides are easily degraded and have a short half-life, limiting the widespread use of OH30.[29–32]

As a new nanomaterial, graphene oxide (GO) has excellent mechanical properties and large specific surface area. GO has also shown superior performance in the treatment of multidrug-resistant bacteria.As a drug delivery carrier, GO can achieve slow release and improve bioavailability.[33] GO conjugated with polyethylene glycol (PEG) also termed PEGylation, is characterized by good biocompatibility, stability, low cytotoxicity, and drug-delivery capability, so it is attracting considerable research attention.[34,35] Drugs can be delivered in many ways, including covalent crosslinking, π–π conjugation, electrostatic adsorption, and disulfide bonding.[36–38] Research has shown that GO can protect protein peptides from protease hydrolysis by stabilizing its biological activity, but ordinary GO has poor stability in various physiological solutions, it is easy to reunite precipitation.The PEG modification of GO can improve its stability in various physiological solutions and its biocompatibility. Research has shown that GO can protect proteins and peptides from protease hydrolysis and thus stabilize their biological activity.[39–41]

In the present study, we used polyethylene GO through the π–π conjugate carrying OH30 to overcome the short half-life and easy inactivation and degradation characteristics of OH30 and promote infective-wound healing.

# Materials and Methods

## Materials

GO sheets were obtained from XFNANO Materials (Nanjing, China). PEG (MW: 10000) was obtained from Fan Shuo (Shanghai, China).

N-(3-Dimethylaminopropyl)-N′-ethylcarbodiimide hydrochloride (EDC) was purchased from Sigma. OH30 was synthesized by GL Biochem (Shanghai) Ltd. Fetal bovine serum (FBS) was purchased from BD. F12 Cell medium, phosphate buffer, trypsin, and MTT were purchased from Solarbio (Beijing, China). All other reagents were purchased from Sinopharmaceutical Co., Ltd. Ultrapure water was used throughout the experiments.

## Cell Culture

HaCaT cells and Human Umbilical Vein Endothelial Cells (HUVECs) were purchased from Kunming Cell Bank of Type Culture Collection (Kunming Institute of Zoology, CAS).HaCaT cells and HUVECs were cultured in F12 and DMEM medium with 10% fetal FBS and 1% penicillin/streptomycin at 37°C in 5% $CO_2$ atmosphere.

## Synthesis of GO-PEG

GO nanosheets were dispersed in water under ultrasonication and then modified into carboxyl-GO (GO-COOH) according to a previously reported experimental method.[42] Then, GO-PEG was obtained by coupling PEG to the carboxyl groups with the help of EDC under ultrasonication. After removing free PEG and EDC by filtration, GO-PEG was obtained.

## Synthesis of PGO-OH30

In order to obtain PGO-OH30,OH30 was added to GO-PEG solution by suspension drop method, and then violently stirred for 12h at room temperature. Free OH30 was removed using an ultrafiltration tube with a 100 kDa molecular weight cutoff. PGO-OH30 was trapped in the ultrafiltration tube and resuspended with water after three to five times of washing.

## Stability in Physiological Solution

Before using GO-PEG for further application, its stability in physiological solution was ensured. In a typical procedure, 0.5 mL each of GO, GO-PEG, and PGO-OH30 was mixed with 0.5 mL each of water, 9% saline (wt/vol), medium, and serum. The GO and GO-PEG samples were centrifuged at 10000g for 5 min at room temperature.

## FTIR Spectroscopy

The formation or evolution of new bonds and surface modification of nanoparticles can be assessed by FTIR spectroscopy. Infrared (IR) absorption spectra were recorded within the range of 800–4000 $cm^{-1}$. Solid samples were prepared by potassium bromide tablet method. Samples were mixed separately with potassium bromide and dried in a constant-temperature oven at 60 °C. Then, the mixture was added to the tablet mold, pressed into a transparent sheet under pressure, and detected with an FTIR spectroscopy system (Thermo, IS10, Shanghai, China). All operations were performed in an IR oven to prevent moisture absorption. The background of KBr was deducted as blank.

## Atomic Force Microscopy (AFM)

The dimensions and thickness of nanosheets were characterized with an AFM system (Agilent 5400 AFM,CA, USA) in tapping mode. Samples were prepared according to a previously reported method.[43] In a typical procedure, GO and GO-PEG were deposited onto silicon wafers as a substrate after being dried naturally.

## Transmission Electron Microscopy (TEM)

The morphology and size of GO and GO-PEG were analyzed by TEM using a Hitachi transmission electron microscope.The samples were diluted with ultrapure water. The diameter of the copper mesh (provided by Hitachi) used in the experiment was 3 mm, provided by Hitachi. The samples were added to the copper mesh with a micropipette, and observed under a transmission electron microscope after natural drying.

## Encapsulation Efficiency (EE%) and Drug-Loading Efficiency (LE%) of OH30

To determine OH30 release and loading efficiency, free peptide was detected by HPLC on a Supersil ODS2 column (Thermofisher, USA).The EE% and LE% of OH30 were calculated using formulas (1) and (2), respectively.

$$EE\%=(OH30_t - OH30_f)/OH30t \times 100 \quad (1)$$

$$LE\%=(OH30_t - OH30_f)/PGO\text{-}OH30_w \times 100 \quad (2)$$

where $OH30_t$ is the total amount of OH30, $OH30_f$ is the free amount of OH30 in the supernatants, and PGO-$OH30_w$ is the total weight of PGO-OH30.

## Drug-Release Behavior

To investigate the drug-release behavior of PGO-OH30, PGO-OH30 was placed in a 100 kDa ultrafiltration device and immersed in 5 mL of PBS (pH 7.4). Then, the release systems were incubated at 37 °C. After centrifugation, the supernatants were obtained at 0.5, 1, 2, 3, 4, 6, 8, 10, 12, and 24 h and replaced with an equal volume of PBS. OH30 was released from PGO-OH30 and detected by HPLC.

## In vitro Bacteriostasis Experiment

To determine if the OH30 released by PGO-OH30 still had antibacterial activity, *S. aureus* ($5 \times 10^4$ CFU/mL) was used to evaluate the antibacterial activity of OH30 released at different times on a 96-well plate. After 24 h of incubation, absorbance was detected at 570 nm with a microplate reader, and then the bacterial inhibition rates at different times were obtained.

## In vitro Cytotoxicity

The cytotoxicity of OH30, GO-PEG, and PGO-OH30 against HaCaT cells was evaluated by MTT assay. In a typical procedure, cells at the logarithmic growth phase were added to 96-well culture plates at $5 \times 10^4$ cells $mL^{-1}$ and 100 μL per well. The plates were incubated 37 °C and 5% $CO_2$ overnight for 24 h with F12 medium containing various concentrations (from 1 μg $mL^{-1}$ to 100 μg $mL^{-1}$) of OH30, GO-PEG, and PGO-OH30. Cell viability was investigated by MTT assay.

## In vitro Cell Migration

Cell-migration assay was performed through a previous method. In a typical procedure, HaCaT cells ($5 \times 10^5$ per well) were seeded onto a six-well plate and grown to 80% confluence. The scratch was created using a sterile pipette tip. The suspended cells were gently washed twice with PBS, and then various serum-free F12 media (50 μg/mL OH30, 50 μg/mL GO-PEG, 50 μg/mL PGO-OH30, and untreated) were added into a six-well plate, which was cultured for additional periods (from 0 h to 48 h). Micrographs were captured

using a microscope (Olympus) at 0, 12, 24, and 48 h after scratch wounding.[44] Cell-migration rate from 0 to 48 h was calculated with Image J.

## Angiogenesis Activity of PGO-OH30

To evaluate the effect of PGO-OH30 on angiogenesis, HUVEC MTT assay and cell-scratch assay were performed. OH30, GO-PEG, and PGO-OH30 (concentrations from 1 μg $mL^{-1}$ to 100 μg $mL^{-1}$) were incubated with HUVEC for 24 h, and the effect of cell viability was evaluated by MTT method. The effect of OH30, GO-PEG, and PGO-OH30 (50 μg/mL) on HUVEC migration was evaluated by cell-scratch assay, and the migration status of HUVECs at 0, 12, 24, and 48 h after scratching was recorded with a microscope.

## Wound-Healing Activity of PGO-OH30

KM mice were obtained from the JiNan PengYue Animal Center (female, 4 weeks of age, and weighing 18–22 g on average). Animals were fed a standard diet and allowed water ad libitum.Each cage contained four mice. After the mice were anesthetized with 4% chloral hydrate, a wound was created using a perforator on the skin of the mouse's back, and then 50 μL of *S. aureus* (ATCC6583) suspension ($2.0 \times 10^7$ CFU/mL) was used to infect the tissue of all mice to establish an experimental model of infection. The mice were randomly divided into five groups: control, positive control (penicillin), GO-PEG, OH30, and PGO-OH30. Each group included 25 mice. Mice that did not fit the normal distribution were excluded from the data analysis. The mice in each group were separately bred, and each group was treated every 24 h. The morphology during the wound-healing process was recorded with a Nikon camera. Skin tissue was obtained after mice were euthanized at days 3, 7, 14, and 21. Wound counting of bacteria, HE staining, and Masson's trichrome staining were performed. All animal procedures, care, and handling were approved by the Ethics Committee of Kunming Institute of Zoology at the Chinese Academy of Sciences or Weifang Medical University. Animal welfare according to the eighth edition of the Guide for the Care and Use of Laboratory Animals (Institute for Laboratory Animal Research. 2011, Washington, DC, USA: National Academies Press) was followed.

# Results

## Synthesis and Characterization of PGO-OH30

PEG was conjugated with GO by the formation of amide bonds under the catalysis of EDC. The GO-PEG structure was confirmed by IR and stability in physiological solution. GO-PEG was vigorously stirred with OH30 to obtain PGO-OH30. PEGylation improved the GO physiological stability and biocompatibility. GO-PEG showed excellent stability in high-concentration salt solution, especially in serum environment (Figure 1A).The experimental results of FTIR showed that the peaks at ~2900 and ~1100 $cm^{-1}$ in the GO-PEG sample were the signatures of C-H and C-O bonds in PEG. The peaks at ~3280 and ~1531 $cm^{-1}$ in the PGO-OH30 sample were the signatures of C-0 and-NH bonds in OH30. The peak at ~815 $cm^{-1}$ suggested that OH30 was linked with GO-PEG through π–π conjugation (Figure 1B and Table 1). AFM is a reliable experimental method for evaluating the size, height, and morphology of GO-derived materials. AFM images indicated that GO had an average diameter of about 200 nm and a thickness of about 1 nm. After PEGylation, the sizes decreased and the thickness of GO-PEG became nearly 1.5 nm, confirming successful modification. After loading OH30, the thickness of PGO-OH30 was approximately 3 nm (Figure 1C).The morphology and size of the results obtained by TEM were consistent with the AFM images (Figure 1D). Zeta potential and size were evaluated with a Marvin laser granulometer, which showed that GO had a negative charge and became less electronegative after modification with PEG. After loading with OH30, the potential of GO was reversed and it became positively charged, which facilitated cellular uptake (Table 2).

## Drug Loading and Release

To achieve high drug loading and entrapment rate, we used OH30 and GO-PEG in different ratios for experiments. Results showed that when the concentrations were 2 mg/mL OH30 and 0.6 mg/mL GO-PEG, LE% reached 70.18% ± 0.93% and EE% reached 77.87% ± 2.22% (Tables 3 and 4). As shown in Figure 2, we evaluated the drug-release behavior in vitro of PGO-OH30. The rapid release of OH30 in 2 h can kill bacteria in the wound, consistent with our expectations. It was then slowly released and reached its peak of about 60% in 12 h, also consistent with a previous report.[20,21]

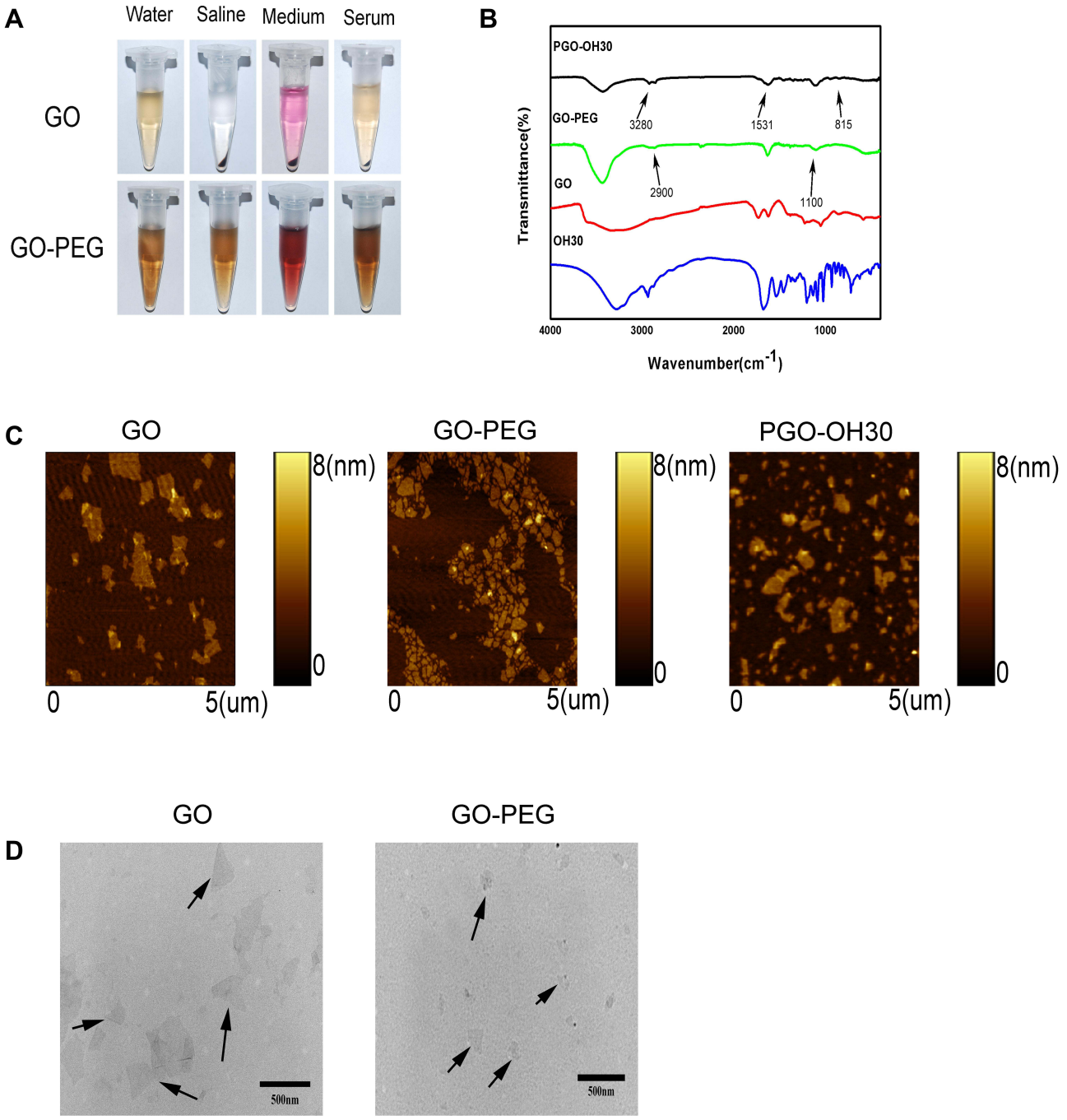


**Figure 1** Characterization of nanomaterials based on graphene oxide. (**A**) Photos of GO and GO-PEG in different physiological solutions (water, saline, medium, and serum) recorded after centrifugation at 10 000g for 5 min. (**B**) FTIR spectra of GO, GO-PEG, OH30, and PGO-OH30. (**C**) AFM images of GO, GO-PEG, and PGO-OH30 in tapping mode. (**D**) TEM images of GO and GO-PEG.The black arrows indicate GO and GO-PEG in the TEM field, respectively.
**Abbreviations:** GO, graphene oxide; GO-PEG, PEGylated graphene oxide; OH30, OH-CATH30; PGO-OH30, PEGylated graphene oxide loaded with OH30.

## In vitro Bacteriostasis Experiment

In vitro bacteriostatic tests of OH30 released by PGO-OH30 (Figure 3) showed that the inhibitory rate of OH30 released at 0.5 h could reach over 73% to *S. aureus*, and the inhibitory rate of OH30 released at 3 h could reach over 95%. Thus, the long-term high inhibitory concentration could be maintained.

**Table 1** Absorption Peak Position of Different Functional Groups in the Infrared Spectrum

| Functional Groups | Absorption Peak ($cm^{-1}$) |
|---|---|
| CO | ~2900 |
| CH | ~1100 |
| NH–CO | ~3280/~1531 |
| π-π conjugate | ~815 |

**Table 2** Particle Zeta Potential and Size of GO,GO-PEG, and PGO-OH30 (Mean ± SD, *n* = 6)

| Sample | Zeta Potential (mV) | Size (nm) | PDI |
|---|---|---|---|
| GO | −24.03±0.29 | 235.27±7.26 | 0.23±0.01 |
| GO-PEG | −5.90±1.01 | 99.98±0.30 | 0.20±0.01 |
| PGO-OH30 | 26.03±1.44 | 106.15±0.95 | 0.19±0.01 |

**Abbreviations:** GO, graphite oxide; GO-PEG, PEGylated graphite oxide; PGO-OH30, PEGylated graphite oxide loaded with OH30; PDI, polydispersity index.

**Table 3** Optimization of Loading Capacity and Encapsulation rate.The Loading Efficiency and Encapsulation Rate of GO-PEG Were Detected by HPLC, and Different Proportions of GO-PEG and OH30 Were Mixed to Obtain Better Loading Efficiency and Encapsulation Rate (Mean ± SD, *n* =3)

| Ratio of OH30 and GO-PEG | Loading Efficiency(%) | Encapsulation Efficiency (%) |
|---|---|---|
| 0.1mg/ml GO-PEG +0.4mg/ml OH30 | 55.15±3.30 | 30.71±3.64 |
| 0.1mg/ml GO-PEG +0.6mg/ml OH30 | 61.69±0.99 | 26.87±1.15 |
| 0.1mg/ml GO-PEG +1mg/ml OH30 | 69.56±0.93 | 22.89±0.99 |
| 0.1mg/ml GO-PEG +2mg/ml OH30 | 80.83±1.15 | 20.47±2.45 |
| 0.1mg/ml GO-PEG +2.5mg/ml OH30 | 79.88±0.11 | 13.0±0.31 |

**Abbreviations:** GO-PEG, PEGylated graphite oxide; OH30, OH-CATH30.

## In vitro Cell Cytotoxicity and Migration

We used MTT to evaluate Hacat cell viability and toxicity after incubation with drug for 24 h. Results (Figure 4) showed that GO-PEG and PGO-OH30 had high cell viability and low toxicity. After GO-PEG was loaded with OH30, the cytotoxicity of OH30 decreased. Thus, PGO-OH30 had good biocompatibility and low cytotoxicity to HaCaT cells. Cell migration plays an important role in wound healing, so we used the scratch test to evaluate the effect of OH30, GO-PEG, and PGO-OH30 on cell migration. As shown in Figures 5A and B, compared with the untreated group, 50 μg/mL PGO-OH30 showed better migration effects on HaCaT cells.

**Table 4** Optimization of Loading Capacity and Encapsulation Rate.The Loading Efficiency and Encapsulation Rate of GO-PEG Were Detected by HPLC, and Different Proportions of GO-PEG and OH30 Were Mixed to Obtain Better Loading Efficiency and Encapsulation Rate (Mean ± SD n = 3)

| Ratio of OH30 and GO-PEG | Loading Efficiency(%) | Encapsulation Efficiency(%) |
|---|---|---|
| 2mg/ml OH30+0.1mg/ml GO-PEG | 80.83±0.49 | 20.47±2.45 |
| 2mg/ml OH30+0.4mg/ml GO-PEG | 72.19±0.99 | 51.93±1.28 |
| 2mg/ml OH30+0.6mg/ml GO-PEG | 70.18±0.93 | 77.87±2.22 |

**Abbreviations:** GO-PEG, PEGylated graphite oxide;OH30, OH-CATH30.

## Angiogenesis Activity of PGO-OH30

HUVECs were used to evaluate the effect of PGO-OH30 on angiogenesis. MTT assay and cell-scratch assay were used to evaluate the effect of PGO-OH30 on HUVEC proliferation and cell migration. Results showed that compared with the control group, PGO-OH30 did not promote the proliferation of HUVECs but promoted cell migration (Figures 6 and 7). Therefore, OH30 and PGO-OH30 may promote skin angiogenesis during wound healing by promoting HUVEC migration.

## Wound-Healing Assays in vivo

The wound-healing process on days 0, 3, 7, and 14 are shown in (Figure 8A and B). The wound-healing speed of

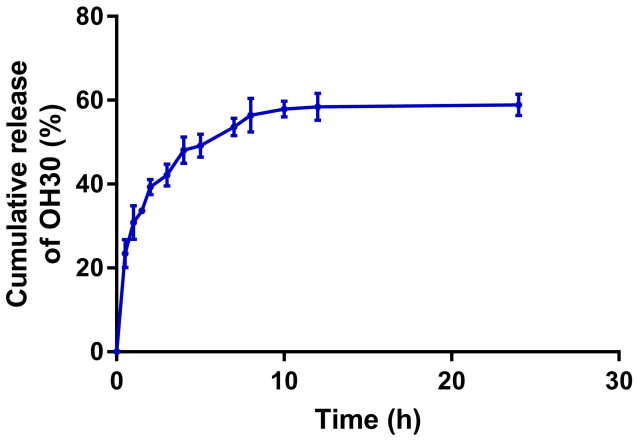


**Figure 2** In vitro drug-release profile of PGO-OH30 at pH 7.4.PO-OH30 was incubated at 37 °C, and OH30 released from PGO-OH30 was detected by HPLC. Data are represented as the mean ± SD, n = 3.
**Abbreviation:** PGO-OH30, PEGylated graphene oxide loaded with OH30.

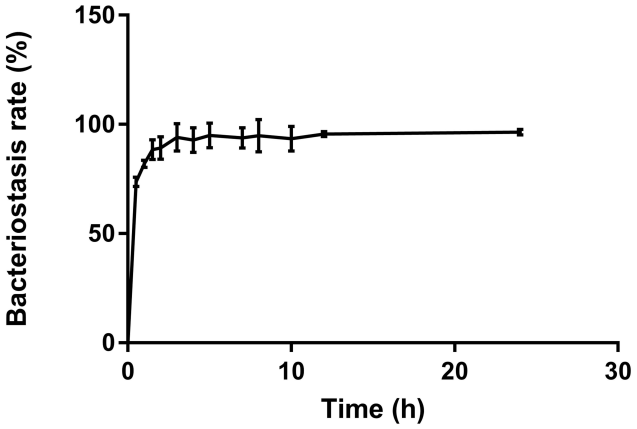


**Figure 3** In vitro antibacterial experiment. The OH30 released at different time points were incubated with *S. aureus*, and the initial bacterial amount was $5\times10^4$ CFU/mL, After 18–24 h of incubation, the bacteriostatic rate was calculated by the OD value. Data are represented as the mean ± SD, n = 3.
**Abbreviations:** PGO-OH30, PEGylated graphene oxide loaded with OH30.

the PGO-OH30 group was faster than those of the other groups, especially on day 7. Results of quantification of bacterial load in the wound suggested that PGO-OH30 can more efficiently remove bacteria from the area around the wound. On day 7, the number of *S. aureus* in wounds of the PGO-OH30 group was 140 times, 14 times, and 6 times less than those in the control, positive control, and OH30 groups (Figure 8C). HE tissue dyeing showed that compared with the control group, the skin-surface layer of the PGO-OH30 group was smoother, and inflammatory-cell infiltration was less. Masson's trichrome staining showed that the newly generated collagen in the wound of the PGO-OH30 group was more regular and more abundant (Figure 9).

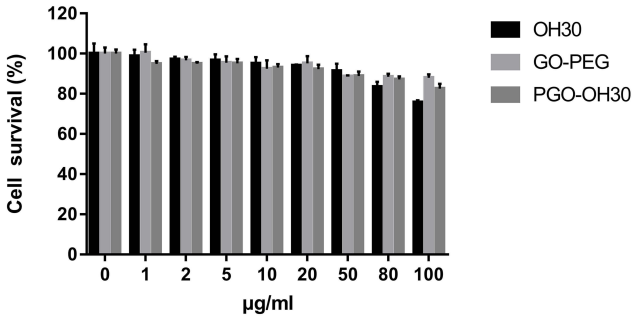


**Figure 4** Cytotoxicity of HaCaT. HaCaT cells were incubated with different concentrations of OH30, GO-PEG, and PGO-OH30 for 24 h. Data are represented as the mean ± SD, n = 3.
**Abbreviations:** GO-PEG, PEGylated graphene oxide; OH30, OH-CATH30; PGO-OH30, PEGylated graphene oxide loaded with OH30 (mean ± SD, *n* = 3).

## Discussion

Bioactive peptides from natural plants and animals have become important candidate molecules for the development of novel antimicrobial drugs.[45] The antimicrobial peptides of the cathelicidin family play an important physiological role, such as bactericidal, immunoregulation and others. OH30 is a small molecular weight antimicrobial peptide from the cathelicidin family of the king cobra, which possesses high efficiency and broad antimicrobial activity without significant hemolytic activity.[10,13,25] At the same time, OH30 also showed good antimicrobial activity against a variety of clinically isolated drug-resistant bacteria, and significantly improved the survival rate of mice in the bacterial infection mouse model.[39] It can selectively upregulate the production of chemokines and cytokines without causing harmful immune reactions, thereby regulating the inflammatory response, and can treat various bacterial infections.[46] Besides, OH30 benefit nonscar wound healing by rebalancing the immune response to the wound to create an anti-inflammatory microenvironment around the wound.[1]

As a polymer with good hydrophilicity, PEG is widely used to chemically modify various nanomaterials, improve the biocompatibility of materials, reduce toxic and side effects, reduce non-specific adsorption in solution environment, reduce immunogenicity, increase physical, chemical and biological stability, and extend the circulating half-life in vivo.[23,43,47] Compared with other modification strategies, such as cationic polymer polyetherimide, PEG modification showed better biocompatibility and lower cytotoxicity, which could improve the safety of graphene for biomedical applications.[23,43]

In this study, we modified GO with PEG and successfully loaded OH30 onto GO-PEG. The prepared nanoparticles have high drug loading capacity and good sustained-release property, which can be released continuously for 12h. PGO-OH30 has good biocompatibility and has no obvious cytotoxicity to HaCaT and HUVEC cells. The experimental results of infected skin wound model showed that PGO-OH30 can accelerate the healing of infected skin wounds, and can promote the clearance of *S. aureus* near the wounds to create a less bacterial healing environment.

Although OH30 plays many important biological functions, its exact receptor and mechanism are still unknown. Studies have reported that human cathelicidin antimicrobial peptide LL37 can exert activity by acting on a variety of molecules on cells, such as P2X7, CXCR2 or

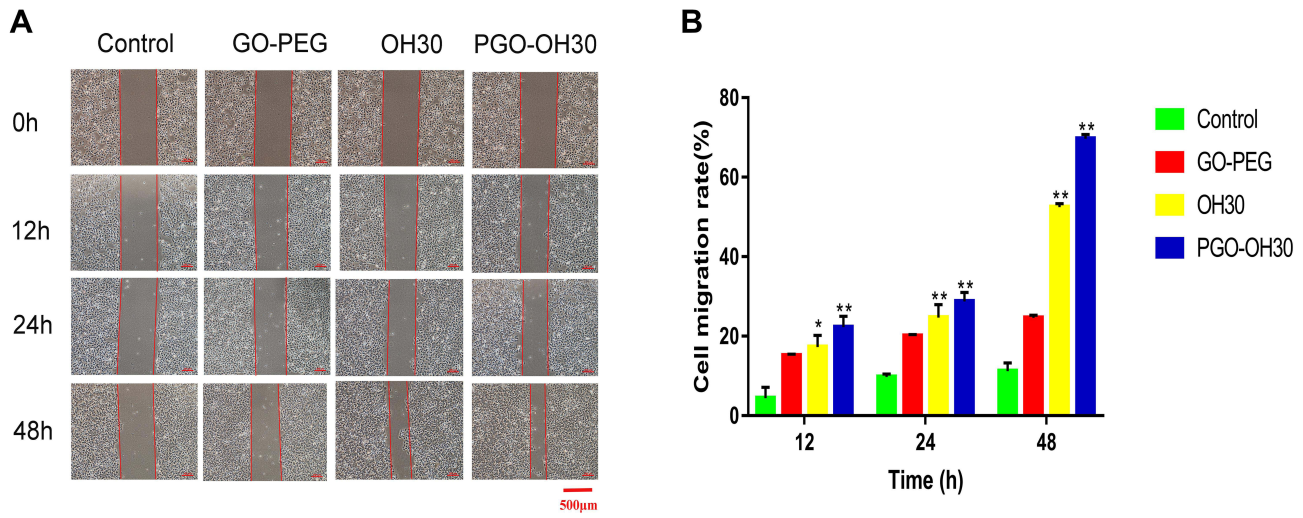


**Figure 5** Effect of GO-PEG, OH30, and PGO-OH30 on cell migration. (**A**) Cell-migration rate from 0 to 48 h. (**B**) Cell-migration rate from 0 h to 48 h calculated with Image J (mean ± SD, n = 3; **P*<0.05 and ***P*<0.01) .

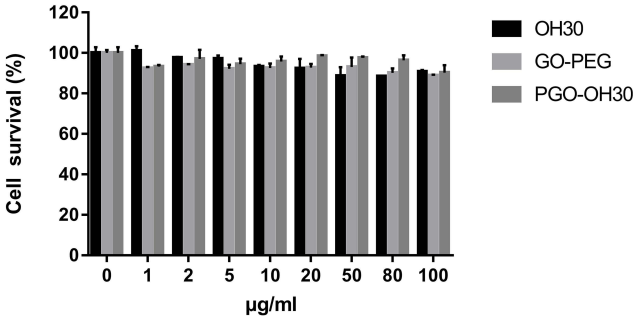


**Figure 6** Cytotoxicity of HUVEC. HUVECs were incubated with different concentrations of OH30, GO-PEG, and PGO-OH30 for 24 h. Data are represented as the mean ± SD, n = 3.
**Abbreviations:** GO-PEG, PEGylated graphene oxide; OH30, OH-CATH30; PGO-OH30, PEGylated graphene oxide loaded with OH30.

GAPDH.[48–50] Therefore, as a homologous molecule of LL37, whether OH30 acts on the above receptor will be an interesting research work in the future.

## Conclusions

We constructed a drug-delivery system based on PEGylated GO to overcome the characteristics of OH30 inactivation and degradation by protease. Cell and animal experiments showed that PEGylated GO loaded with OH30 had good biocompatibility and low cytotoxicity, thereby promoting the healing of infectious skin wounds. This drug-delivery system had high drug-

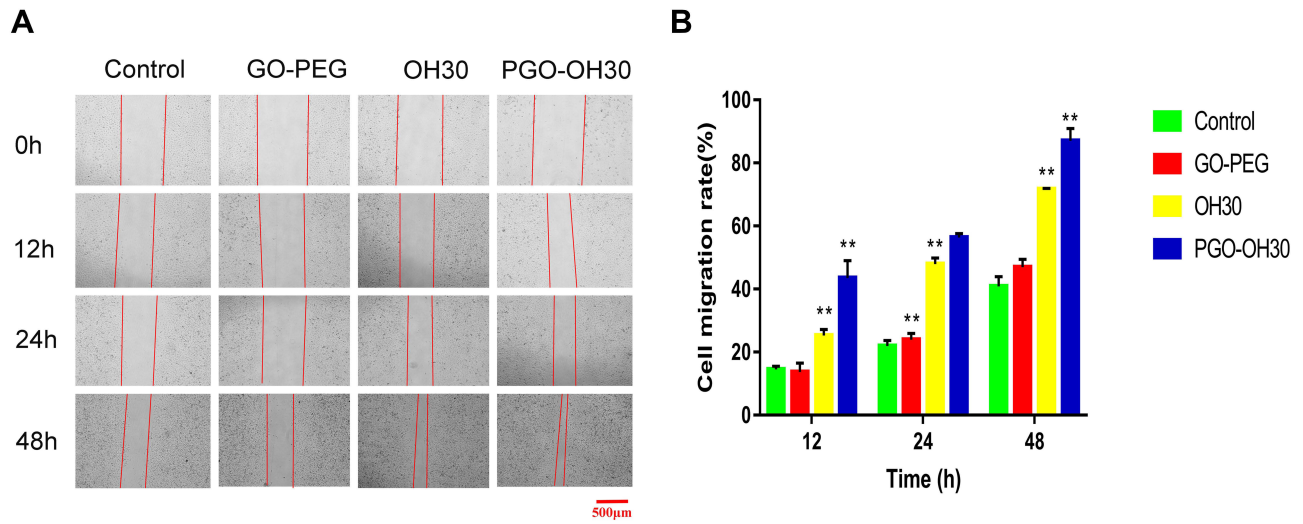


**Figure 7** Effect of GO-PEG, OH30, and PGO-OH30 on cell migration. (**A**) Cell-migration rate from 0 h to 48 h. (**B**) Cell-migration rate from 0 to 48 h calculated with Image J.
**Notes:** (mean ± SD, n = 3, ***P*<0.01).
**Abbreviations:** GO-PEG, PEGylated graphene oxide; OH30, OH-CATH30; PGO-OH30, PEGylated graphene oxide loaded with OH30.

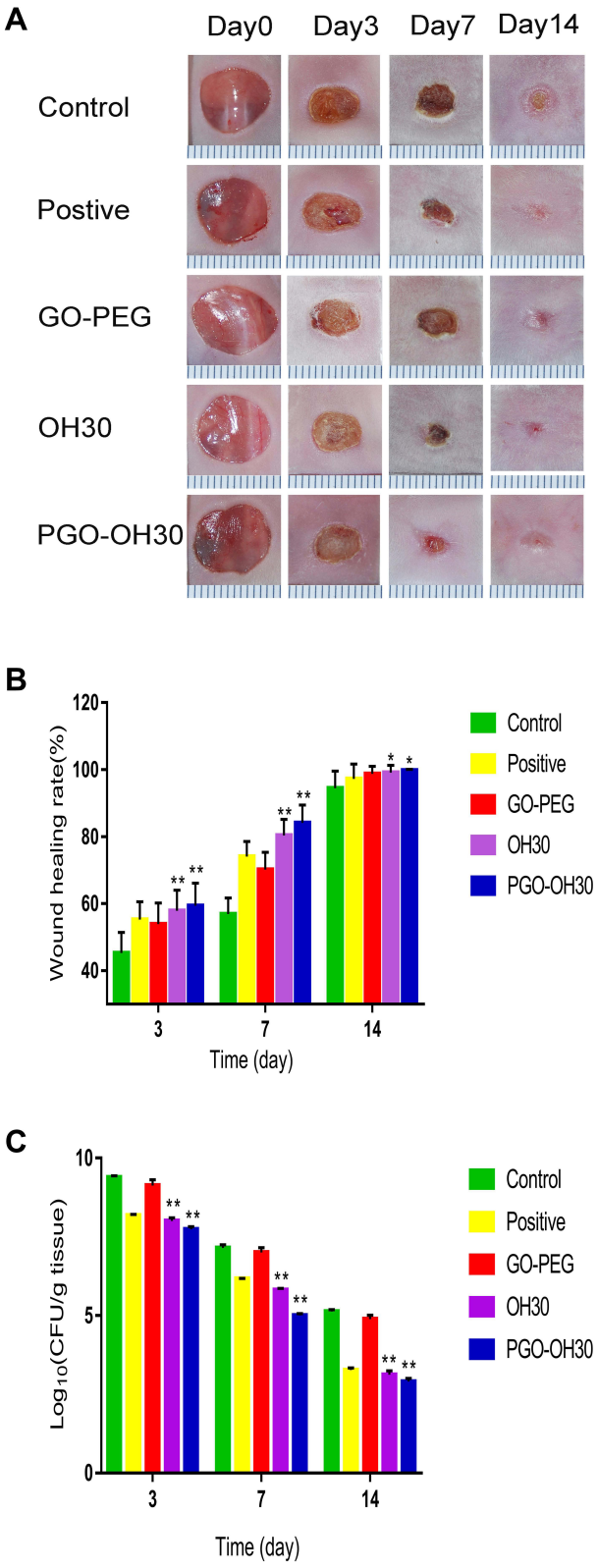


**Figure 8** PGO-OH30 promoted the rapid skin-wound repair. (**A**) Mice with wounds after *S. aureus* infection were treated with saline, GO-PEG, OH30, or PGO-OH30, respectively. Mouse wound closure on days 3, 7, and 14 was recorded with a camera, and the representative photographs are presented. (**B**) Wound-healing rate in mice was quantitative analyzed by calculating the area of the wound on days 3,7, and 14. Bars represent the mean ± SD from three replicates. **P*<0.05, ***P*<0.01 vs. control by using one-way ANOVA (n = 8). (**C**) Quantification analysis of bacterial load in the wound on days 3,7, and 14. Bars represent the mean ± SD from three replicates. ***P*<0.01 vs. control by using one-way ANOVA (n = 8). All data are representative of at least three independent experiments.

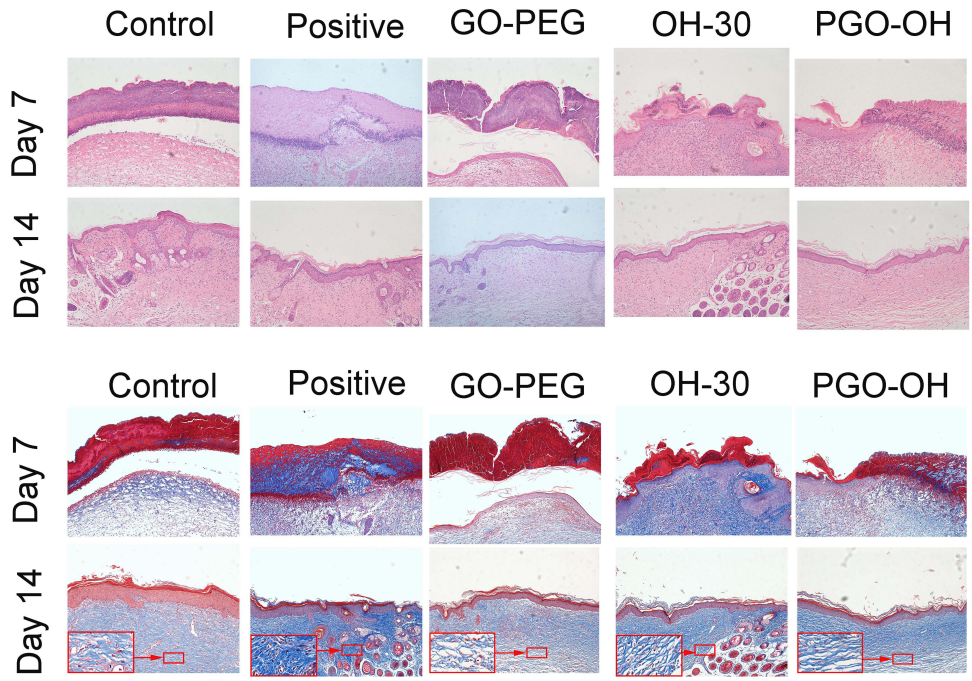


**Figure 9** Skin samples were prepared on days 7 and 14 after mice were treated with GO-PEG, OH30, or PGO-OH30. Then, H&E and Masson staining were performed to analyze pathological changes in the skin.

delivery capability and good biocompatibility. Thus, the drug-delivery system based on PEGylated graphene has great application prospects in solving the problem of short half-life of various peptides. However, the use of GO as a drug carrier remains in the research stage and many problems need to be solved. For example, in terms of biological safety, some conclusions are still controversial, including those on the toxicity of normal cells in the body, metabolism and excretion process in the body, and a series of physiological and biochemical reactions triggered by entering the body and their mechanism of action.

## Acknowledgments

This work was supported by the Youth Innovative Team Development Plan of Universities in Shandong Province (2019KJM003) and Natural Science Foundation of Shandong Province (ZR201807090175).

## Disclosure

The authors report no conflicts of interest in this work.

## References

1. Tongyi S, Zhan B, Zhang W, et al. Carboxymethyl chitosan nanoparticles loaded with bioactive peptide OH-CATH30 benefit nonscar wound healing. *Int J Nanomedicine*. 2018;13:5771
2. Poustchi F, Amani H, Ahmadian Z, Niknezhad SV, Shahbazi MA. Combination Therapy of Killing Diseases by Injectable Hydrogels: From Concept to Medical Applications. Adv Healthcare Mater. 2020;10(3):2001571.
3. Evelina V, Ö E, Anneleen M, et al. Accelerated wound healing in mice by on-site production and delivery of CXCL12 by transformed lactic acid bacteria. *Proc Natl Acad Sci U S A*. 2018;115:8.
4. Diana O, Anabela B, Manuel S. Staphylococcus aureus Toxins and Their Molecular Activity in Infectious Diseases. *Toxins*. 2018;10:6.
5. Wu GS, Zhu BH, Hong XD, Luo PF, Xia ZF. Role of cytokines in host defense against Staphylococcus aureus skin infection. *Histol Histopath*. 2017;32(8):761–766.
6. Tottoli EM, Dorati R, Genta I, Chiesa E, Pisani S, Conti B. Skin wound healing process and new emerging technologies for skin wound care and regeneration. *Pharmaceutics*. 2020;12(8):30. doi:10.3390/pharmaceutics12080735
7. Jarraud S, Cozon G, Vandenesch F, Bes M, Lina G. Involvement of Enterotoxins G and I in staphylococcal toxic shock syndrome and staphylococcal scarlet fever. *J Clin Microbiol*. 1999;37(8):2446–2449. doi:10.1128/JCM.37.8.2446-2449.1999
8. Sophie J, Christophe M, Jean T, et al. Relationships between Staphylococcus aureus genetic background, virulence factors, agr groups (alleles), and human disease. *Infect Immun*. 2002;70:2.
9. Shamez L. Understanding the mechanism of action of the exfoliative toxins of Staphylococcus aureus. *FEMS Immunol Med Microbiol*. 2003;(2):181–189.
10. Li SA, Lee WH, Zhang Y. Efficacy of OH-CATH30 and Its analogs against drug-resistant bacteria in vitro and in mouse models. *Antimicrob Agents Chemother*. 2012;56(6):3309–3317. doi:10.1128/AAC.06304-11
11. Zhang L, Parente J, Harris SM, Woods DE, Hancock REW, Falla TJ. Antimicrobial Peptide Therapeutics for Cystic Fibrosis. *Antimicrob Agents Chemother*. 2005;49(7):2921–2927. doi:10.1128/AAC.49.7.2921-2927.2005

12. Brogden KA. Antimicrobial peptides: pore formers or metabolic inhibitors in bacteria? *Nat Rev Microbiol*. 2005;3:3. doi:10.1038/nrmicro1098
13. Zou P, Lee WH, Gao Z, Qin D, Gao Y. Wound dressing from polyvinyl alcohol/chitosan electrospun fiber membrane loaded with OH-CATH30 nanoparticles. *Carbohydr Polym*. 2019;232:115786. doi:10.1016/j.carbpol.2019.115786
14. Pandey AT, Pandey I, Zamboni P, Gemmati D, Singh MP. Traditional herbal remedies with a multifunctional therapeutic approach as an implication in COVID-19 associated co-infections. *Coatings*. 2020;10(8):761. doi:10.3390/coatings10080761
15. Pandey AT, Pandey I, Hachenberger Y, Krause BC, Singh AV. Emerging paradigm against global antimicrobial resistance via bio-prospecting of mushroom into novel nanotherapeutics development. *Trends Food Sci Technol*. 2020;106(December 2020):333–344. doi:10.1016/j.tifs.2020.10.025
16. Li X, Fan R, Tong A. In situ gel-forming AP-57 peptide delivery system for cutaneous wound healing. *Int J Pharm*. 2015;495(1):560–571. doi:10.1016/j.ijpharm.2015.09.005
17. Duch MC, Budinger GRS, Liang YT, et al. Minimizing oxidation and stable nanoscale dispersion improves the biocompatibility of graphene in the lung. *Nano Lett*. 2011;11(12):5201. doi:10.1021/nl202515a
18. Di GA, Floriana C, Akiko I, et al. The frog skin-derived antimicrobial peptide Esculentin-1a(1-21)NH2 promotes the migration of human HaCaT Keratinocytes in an EGF receptor-dependent manner: a novel promoter of human skin wound healing? *Plos One*. 2015;10(6):e0128663. doi:10.1371/journal.pone.0128663
19. Liu, Mu L, Tang J, et al. A potential wound healing-promoting peptide from frog skin. *Int J Biochem Cell Biol*. 2014;49:32–41.
20. Qiao Y, Ping Y, Zhang HB, et al. Laser-activatable CuS nanodots to treat multidrug-resistant bacteria and release copper ion to accelerate healing of infected chronic nonhealing wounds. *ACS Appl Mater Interfaces*. 2019;11(4):3809–3822. doi:10.1021/acsami.8b21766
21. Elshamy AA, Aboshanab KM. A review on bacterial resistance to carbapenems: Epidemiology, detection and treatment options. *Future ence OA*. 2020;6(3):FSO438. doi:10.2144/fsoa-2019-0098
22. Wu L, Wang JS, Feng LY, Ren JS, Wei WL, Qu XG. Label-Free Ultrasensitive Detection of Human Telomerase Activity Using Porphyrin-Functionalized Graphene and Electrochemiluminescence Technique. *Adv Mater*. 2012;24(18):2447–2452. doi:10.1002/adma.201200412
23. Liu Z, Robinson JT, Sun X, Dai H. PEGylated nano-graphene oxide for delivery of water insoluble cancer drugs. *J Am Chem Soc*. 2008;130(33):10876–10877. doi:10.1021/ja803688x
24. Ronevi T, Puizina J, Tossi A. Antimicrobial peptides as anti-infective agents in pre-post-antibiotic era? *Int J Mol ences*. 2019;20:22.
25. Li SA, Liu J, Xiang Y, Wang YJ, Lee WH, Zhang Y. Therapeutic potential of the antimicrobial peptide OH-CATH30 for antibiotic-resistant pseudomonas aeruginosa keratitis. *Antimicrob Agents Chemother*. 2014;58(6):3144–3150. doi:10.1128/AAC.00095-14
26. Mayandi V, Wen Choong AC, Dhand C. Multifunctional antimicrobial nanofiber dressings containing εpolylysine for the eradication of bacterial bioburden and promotion of wound healing in critically colonized wounds. *ACS Appl Mater Interfaces*. 2020;12(14):15989–16005. doi:10.1021/acsami.9b21683
27. Gurtner GC, Werner S, Barrandon Y, Longaker MT, Repair W. Regeneration. *Nature*. 2008;453(7193):314–321. doi:10.1038/nature07039
28. Liang Y, Chen B, Li M, He J, Yin Z, Guo B. Injectable antimicrobial conductive hydrogels for wound disinfection and infectious wound healing. *Biomacromolecules*. 2020;21(5):1841–1852. doi:10.1021/acs.biomac.9b01732
29. Zhi M, Han J, Chang B, et al. Membrane-Active Amphipathic Peptide WRL3 with in vitro antibiofilm capability and in vivo efficacy in treating methicillin-resistant staphylococcus aureus burn wound infections. *Acs Infect Dis*. 2017.
30. Lachiewicz AM, Hauck CG, Weber DJ, Cairns BA, Van Duin D. Bacterial infections after burn injuries: impact of multidrug resistance. *Clin Infect Dis Off Publ Infect Dis Soc Am*. 2017;12:2130.
31. Yan H, Teh C, Sreejith S, et al. Functional Mesoporous Silica Nanoparticles for Photothermal-Controlled Drug Delivery In Vivo†. *Angewandte Chem Int Ed*. 2012;51(33):8373–8377.
32. Health UDo, Services H. Antibiotic resistance threats in the United States, 2013; 2013.
33. Singh V, Kumar V, Kashyap S, et al. Graphene oxide synergistically enhances antibiotic efficacy in Vancomycin resistance Staphylococcus aureus. *ACS Applied Bio Mater*. 2019;2(3):1148–57.
34. Singh AV, Maharjan RS, Kanase A, Siewert K, Luch A. Machine-learning -based approach to decode the influence of nanomaterial properties on their interaction with cells. *ACS Appl Mater Interfaces*. 202013(1):1943–55.
35. Mei L, Lu Z, Zhang X, Li C, Jia Y. Polymer-Ag nanocomposites with enhanced antimicrobial activity against bacterial infection. *Acs Appl Mater Interfaces*. 2014;6(18):15813–15821. doi:10.1021/am502886m
36. Singh AV, Rosenkranz D, Ansari M, et al. Artificial intelligence and machine learning empower advanced biomedical material design to toxicity prediction. Advan Intelligent Syst;2(12):2000084.
37. Edwards IA, Elliott AG, Kavanagh AM, Blaskovich MAT, Cooper MA. Structure-Activity and -Toxicity Relationships of the Antimicrobial Peptide Tachyplesin-1. *Acs Infect Dis*. 2017;3(12):917–926. doi:10.1021/acsinfecdis.7b00123
38. Butler MS, Paterson DL. Antibiotics in the clinical pipeline in October 2019. *J Antibiotics*. 2020;73:1.
39. Zhao F, Lan XQ, Du Y, et al. King cobra peptide OH-CATH30 as a potential candidate drug through clinic drug-resistant isolates. *Zoological Res*;2018;39(2):87–96.
40. Satya S, Alison K, McDermott M. Role of host-defence peptides in eye diseases. *Cell Mol Life Sci*. 2011.
41. Silva NC, Sarmento B, Pintado M. The importance of antimicrobial peptides and their potential for therapeutic use in ophthalmology. *Int J Antimicrob Agents*. 2013;41:1. doi:10.1016/j.ijantimicag.2012.07.020
42. Singh AV, Mehta KK, Worley K, Dordick JS, Kane RS, Wan LQ. Carbon nanotube-induced loss of multicellular chirality on micropatterned substrate is mediated by oxidative stress. *Acs Nano*. 2014;8(3):2196–2205. doi:10.1021/nn405253d
43. Zhang L, Xia J, Zhao Q, Liu L, Zhang Z. Functional graphene oxide as a nanocarrier for controlled loading and targeted delivery of mixed anticancer drugs. *Small (Weinheim an der Bergstrasse, Germany)*. 2010;6(4):537–544. doi:10.1002/smll.200901680
44. Singh AV, Kishore V, Santamauro G, Yasa O, Sitti M. Mechanical Coupling of Puller and Pusher Active Microswimmers Influences Motility. *Langmuir*. 2020;XXXX(XXX).
45. Mookherjee N, Anderson MA, Haagsman HP, Davidson DJ. Antimicrobial host defence peptides: functions and clinical potential. *Nat Rev Drug Discov*. 2020;19:5.
46. Sheng-An L, Yang X, Yan-Jie W, Jie L, Wen-Hui L, Yun Z. Naturally occurring antimicrobial peptide OH-CATH30 selectively regulates the innate immune response to protect against sepsis. *J Med Chem*. 2013;56:22.
47. Lp P. Controlled drug delivery carrier of nifedipine using biodegradable microcapsule polymer from Poly (D,L-Lactic Acid) and Polyethylene Glycol. *J Phys Conf Ser*. 2021;1751:1.

48. Yu XR, Quan JJ, Long WL, et al. LL-37 inhibits LPS-induced inflammation and stimulates the osteogenic differentiation of BMSCs via P2X7 receptor and MAPK signaling pathway. *Exp Cell Res*. 2018;372(2):178–187. doi:10.1016/j.yexcr.2018.09.024
49. Verjans ET, Zels S, Luyten W, Landuyt B, Schoofs L. Molecular mechanisms of LL-37-induced receptor activation: An overview. *Peptides*. 2016;85:16–26. doi:10.1016/j.peptides.2016.09.002
50. Mookherjee N, Lippert DND, Hamill P, et al. Intracellular Receptor for Human Host Defense Peptide LL-37 in Monocytes. *J Immunol*. 2009;183(4):2688–2696. doi:10.4049/jimmunol.0802586